EXPLORING IO'S ATMOSPHERIC COMPOSITION WITH APEX: FIRST MEASUREMENT OF $^{34}SO_2$ AND TENTATIVE DETECTION OF KCl

A. MOULLET[1], E. LELLOUCH[2], R. MORENO[2], M. GURWELL[3], J. H BLACK[4], AND B. BUTLER[5]

[1] National Radio Astronomy Observatory, Charlottesville, VA-22902, USA
[2] LESIA-Observatoire de Paris, 5 place J. Janssen, F-92195 Meudon CEDEX, France
[3] Harvard-Smithsonian Center for Astrophysics, Cambridge, MA-02138, USA
[4] Department of Earth and Space Sciences, Chalmers University of Technology, Onsala
Space Observatory, SE-43992 Onsala, Sweden
[5] National Radio Astronomy Observatory, Socorro, NM-87801, USA

ABSTRACT

The composition of Io's tenuous atmosphere is poorly constrained. Only the major species SO_2 and a handful of minor species have been positively identified, but a variety of other molecular species should be present, based on thermochemical equilibrium models of volcanic gas chemistry and the composition of Io's environment. This paper focuses on the spectral search for expected yet undetected molecular species (KCl, SiO, S_2O) and isotopes ($^{34}SO_2$). We analyze a disk-averaged spectrum of a potentially line-rich spectral window around 345 GHz, obtained in 2010 at the APEX 12 m antenna. Using different models assuming either extended atmospheric distributions or a purely volcanically sustained atmosphere, we tentatively measure the KCl relative abundance with respect to SO_2 and derive a range of 4×10^{-4}–8×10^{-3}. We do not detect SiO or S_2O and present new upper limits on their abundances. We also present the first measurement of the $^{34}S/^{32}S$ isotopic ratio in gas phase on Io, which appears to be twice as high as the Earth and interstellar medium reference values. Strong lines of SO_2 and SO are also analyzed to check for longitudinal variations of column density and relative abundance. Our models show that, based on their predicted relative abundance with respect to SO_2 in volcanic plumes, both the tentative KCl detection and SiO upper limit are compatible with a purely volcanic origin for these species.

Key words: planets and satellites: atmospheres – submillimeter: planetary systems

Online-only material: color figures

1. INTRODUCTION

The Galilean moon Io holds a very tenuous atmosphere ($\sim$1–10 nbar pressure at the ground) that is unusual in many respects. This is the only known SO_2-dominated atmosphere ($\sim$90% of the total pressure) and is ultimately dependent upon the volcanic activity of the moon, the most intense in the solar system. The atmosphere acts as a reservoir feeding a plasma torus in orbit around Jupiter that sweeps the upper gas layers at a rate as high as 1 ton s^{-1} (Schneider & Bagenal 2007), thus requiring a continuous and efficient atmospheric replenishment mechanism. It is yet unclear whether the bulk of the dayside atmosphere is replenished directly by the outgassing of volcanic plumes or by sublimation of SO_2 volcanic condensates (see review in Lellouch 2005). The latest results obtained on SO_2 spatial distribution (Feaga et al. 2009; Moullet et al. 2010) and column density variation with heliocentric distance (Tsang et al. 2012) tend to support sublimation as the major immediate source.

Io's atmosphere displays marked longitudinal column density variations on the dayside, by a factor up to 10 along the equator (Spencer et al. 2005). In addition, it is expected that the pressure collapses almost entirely on the nightside and at high latitudes, where the colder surface temperature cannot maintain a significant SO_2 column density through sublimation, except possibly around volcanic centers.

Primarily due to instrumental sensitivity limitations, the composition of Io's atmosphere has been poorly constrained observationally. Beyond SO_2, only three molecular species have been identified in the lower atmosphere:

1. SO is the main expected photochemistry product of SO_2 and was first detected by Lellouch et al. (1996) with an abundance of 3%–10% with respect to SO_2 (i.e., mixing ratio). Measurements of significant temporal variations in the SO mixing ratio, as well as mapping of SO lines emission (de Pater et al. 2007; Moullet et al. 2010) that shows a spatial distribution more localized and linked to volcanic centers than the bulk SO_2 atmosphere, support the hypothesis that atmospheric SO is at least partially sustained by plume outgassing.

2. NaCl has been detected by millimeter spectroscopy (Lellouch et al. 2003) with a mixing ratio of 0.3%–1.3% and could be the main carrier for the Na and Cl ions present in the plasma torus. This molecule has a very short lifetime in the atmosphere due to photolysis and rapid condensation on the surface (Moses et al. 2002). The presence of NaCl in volcanic plumes had been predicted by thermochemical equilibrium models of volcanic gas chemistry (Fegley & Zolotov 2000b). It is expected to be injected in the atmosphere directly through volcanic outgassing or sputtering of Na-bearing volcanic frosts by high-energy particles from Io's torus (Johnson & Burnett 1990), but not sustained via sublimation.

3. S_2 was detected by *Hubble Space Telescope* (*HST*) over the Pele plume (Spencer et al. 2000) with a temporally variable (Jessup et al. 2004) yet significant mixing ratio (8%–33%), hinting at a primarily volcanic origin. As S_2 is expected to quickly condense on the surface, it should remain localized mostly around volcanic centers. On the ground, it could polymerize into S_3 and S_4, which are thought to be responsible for the observed ring-shaped red-colored deposits.

In parallel to these observations, numerous theoretical models predicting the composition of Io's atmosphere have been

Table 1
Io's Observational Parameters at the Time of Observations

Date	Angular Size ($''$)	Central Longitudes ($^\circ$W)	On-source Time (hr)	rms on Spectrum (mK channel^{-1})
2010 Aug 20	1.226	90–150	1.4	15
2010 Aug 21	1.227	293–315	0.5	20
2010 Oct 13	1.247	279–312	0.7	23
2010 Oct 15	1.242	300–329	0.7	23
Combined spectrum	1.226		3.3	9.5

Notes. To obtain the combined spectrum, the antenna temperature scale of the individual scans is rescaled to the same apparent angular size, before averaging all the scans together. The rms is determined by the uncertainty on the spectrum continuum baseline around 344.8 GHz, using the original 122 kHz spectral resolution.

developed. Summers & Strobel (1996) showed that SO_2 photochemistry should produce highly volatile, poorly condensible molecular species in the lower atmosphere such as O_2, SO, S_2, as well as atomic species S and O, that, through atmospheric transport, can build up in the nightside where O_2 and SO may be the main constituents. Surface sputtering could also trigger the production of non-condensible or partially condensible atomic and molecular gases (S, K, Na, NaS, Na_2O, . . .; Wiens et al. 1997; Chrisey et al. 1988; Haff et al. 1981).

An extensive literature focuses on detailed modeling of the composition of the gas mixture expelled by volcanic plumes, for a variety of temperature and pressure conditions in volcanic conduits, as well as different bulk magmatic atomic ratios, resulting in a wide range of expected species and abundances (i.e., Zolotov & Fegley 1998; Fegley & Zolotov 2000b; Moses et al. 2002; Schaefer & Fegley 2004). Assuming bulk magma composition based on Io's plasma torus and chondritic abundances, sulfur- (S_2, S_3, S_2O), carbon- (CO, CO_2, OCS), silicate- (SiO, Si), potassium- (KCl, K), and sodium-bearing molecules and atoms (NaCl, Na), among others, may be present in volcanic plumes at mixing ratios higher than 1×10^{-4}. On the other hand, hydrogen-bearing molecules that are often found in terrestrial plumes (such as H_2O and H_2S) may not be present at significant levels as Io appears to be hydrogen depleted (Fegley & Zolotov 2000a). Many of the volcanic species expected on Io have a short lifetime in the atmosphere due to destruction by photochemical reactions and/or high condensibility on the cold ground ($\sim$90–130 K), thus forming condensate deposits around the plumes. These deposits can be partially re-injected back into the atmosphere by sputtering or, for the more volatile species (such as SO_2), through sublimation.

By relating measurements of the mixing ratios of different species to the above models, one can in principle better characterize volcanic regimes, the interactions of the atmosphere with its environment (surface and plasma torus), as well as check the validity of photochemical models. A more detailed knowledge of the chemical composition of Io's atmosphere, including the detection of expected yet undetected species, is essential for the understanding of the moon as a whole. The study of Io's spectrum in the (sub)millimeter wavelength range, which contains many rotational transitions of species that are or could be present in the atmosphere, is the most promising technique to pursue for the exploration of Io's chemistry, and is now more feasible with the recent developments of very sensitive instruments.

In this paper, we report on a spectroscopic exploration project carried out with the 12 m Atacama Pathinder EXperiment (APEX) antenna coupled with the APEX-2 heterodyne receiver. Spectra were obtained in the summer and fall of 2010 and targeted rotational transitions of confirmed molecules (SO_2,

SO), as well as expected yet undetected species (KCl, SiO, S_2O) and isotopes ($^{34}SO_2$). We describe the data and the models used to derive column densities and mixing ratios. We present the first measurement of the $^{34}S/^{32}S$ isotopic ratio in gaseous SO_2, a tentative detection of KCl, upper limits on SiO and S_2O, and inferences on the role of volcanism for atmospheric replenishment.

2. OBSERVATIONS

The data analyzed in this paper were obtained on the APEX antenna, a 12 m diameter dish located on Llano de Chajnantor, at an altitude of 5100 m, in Chile (Güsten et al. 2006). The observations were performed in 2010 August and October, aggregating a total of $\sim$3.3 hr of on-source integration time (corresponding to $\sim$16.5 total hours of observation, taking into account time on the off position and overheads), with 1.4 hr on the leading hemisphere of Io (eastern elongation, longitudes 0°–180°W), and 1.9 hr on the trailing hemisphere (western elongation, longitudes 180°–360°W). The relevant observational parameters for each observation period are gathered in Table 1.

The single-sideband Swedish Heterodyne Facility Instrument (Lapkin et al. 2008) was tuned to cover the 344.100–345.100 GHz and 346.430–347.430 GHz spectral windows. This setup was designed so as to target at once multiple rotational transitions of different species: two SO_2 transitions (346.523 and 346.652 GHz), two SO transitions (344.310 and 346.528 GHz), one KCl transition (344.820 GHz), one SiO transition (347.330 GHz), five $^{34}SO_2$ transitions (344.245, 344.581, 344.808, 344.987, and 344.998 GHz), and five S_2O transitions (344.851, 346.543, 346.804, 346.862, and 347.123 GHz). The Fast Fourier Transform Spectrometer backend (Klein et al. 2006) provided a spectral resolution of 122 kHz (equivalent to 106 m s^{-1} at 345 GHz), which is sufficient to resolve the Doppler-broadened lines ($\sim$600–800 m s^{-1} width). At the observed frequency, the antenna beam is $\sim$17$''$ and does not resolve Io's disk ($\sim$1$''$.2), so that all the presented measurements are disk-averaged spectra.

The observations were performed in on–off mode, hence in the raw spectra most of the sky thermal contribution is already removed, and the instrumental bandpass response corrected for. We noticed that the continuum level could vary significantly from scan to scan and even reach large negative values; however, line emission above the continuum is not affected by the continuum variations. These variations are probably related to the contribution of a strong continuum source (Jupiter) in the sidelobes. In the scans that are the most affected, the spectra can also display a large variability of the bandpass response on scales of a few hundred MHz (ripples). These issues prevent us from correctly estimating Io's continuum emission level, but

still allow us to measure the emission contrast of each line. To extract the spectra, using the GILDAS-CLASS package,[6] we carefully removed the continuum emission in each scan after fitting the continuum baseline by a polynomial (of order lower or equal to two). A few scans where the continuum level could not be well estimated were flagged and removed. To account for Io's angular size variation from 2010 August to October, we rescaled the 2010 October data by normalizing each scan's antenna temperature to the equivalent antenna temperature for the geocentric distance of 2010 August. We then combined together the obtained scans by averaging them on a common rest frequency scale, taking into account the line-of-sight projected velocity of the source at the time of each scan.

The continuum-subtracted spectrum obtained is measured in the $T_A^\star$ scale, corresponding to the antenna temperature corrected for atmospheric absorption. To convert this scale to a disk-averaged brightness temperature scale, we multiplied the $T_A^\star$ values by the dilution factor (taking into account Io's ephemeris size and the beam size at each frequency), and by the antenna efficiency equal to $B_{\rm eff}/F_{\rm eff}$, where the telescope forward efficiency $F_{\rm eff}$ is estimated at 0.95 and the main-beam efficiency $B_{\rm eff}$ at 0.73 (Güsten et al. 2006). We estimate an error of 5% on the determination of the brightness temperature scale.

After combining all the obtained scans, the rms on the spectrum obtained (combined spectrum) is 9.5 mK at 344.8 GHz on the antenna temperature scale (for each spectral channel), corresponding to 3.8 K in equivalent disk-averaged brightness temperature on Io. When binned to obtain a spectral resolution of 488 kHz (424 m s^{-1} at 345 GHz), closer to the expected line widths, the rms decreases to 4.8 mK (1.9 K in equivalent disk-averaged brightness temperature).

3. ATMOSPHERIC MODELING

3.1. Radiative Transfer

To create synthetic atmospheric disk-averaged lines against which to compare the data, we use a numerical radiative transfer model described in detail in Moullet et al. (2008). For a given transition, considering the local gas temperature, density, and velocity in each cell of a three-dimensional spatial grid encompassing the whole atmosphere, the code computes each local rotational line opacity profile, using spectroscopic parameters retrieved from the Splatalogue catalog[7] and the CDMS database.[8] Pressure broadening of the line profile is neglected at the low pressures considered here, so that the line profiles are assumed to be only thermally and dynamically Doppler-broadened. The brightness temperature corresponding to each line-of-sight direction is then computed through the corresponding atmospheric column, under the assumption that the emission is in local thermodynamical equilibrium. A continuum thermal surface emission at the brightness temperature of 95 K is assumed, corresponding to the average brightness temperature measured at ∼345 GHz (Moullet et al. 2010). The synthetic disk-averaged line is finally derived by summing all local brightness temperatures in the grid and rescaling the result to Io's disk size.

3.2. Extended Atmospheric Distributions (Hydrostatic Case)

We first consider the case of an atmospheric global structure mimicking a horizontally extended atmosphere in hydrostatic

equilibrium—akin to the case of a sublimation-sustained bulk atmosphere. The primary purpose of this modeling work is to determine the disk-averaged SO$_2$ column density and the abundances of the observed minor species with respect to SO$_2$ (i.e., mixing ratios).

We use a computing grid with 30 km resolution in the plane of sky and 0.25 km resolution in altitude. The airmass at each cell is computed assuming plane-parallel geometry. Our atmospheric distribution model assumes that SO$_2$ and all other species are co-located vertically and horizontally. Emission on the limbs, corresponding to the terminator region, is ignored since sublimation is unlikely to support significant amounts of SO$_2$ on the nightside. Otherwise, we assume either a horizontally constant column density d (homogeneous distribution model) or a spatially variable column density, taking as a reference the atmospheric distribution model proposed by Feaga et al. (2009) based on *HST* disk-resolved SO$_2$ observations. The latter model proposes an atmosphere restricted to longitudes lower than 70°, with column densities increasing toward the equatorial region. It also displays significant longitudinal variations (from 1×10^{16} mol cm^{-2} to 5×10^{16} mol cm^{-2} at the equator), with lower column densities on the sub-Jovian hemisphere than on the anti-Jovian hemisphere. We utilize the Feaga model distribution as a reference for relative column density variations across the disk, but allow the overall distribution to be scaled by a single parametric factor χ.

For both homogeneous and Feaga distribution models, the vertical density profile within each atmospheric column is computed assuming hydrostatic equilibrium, using the SO$_2$ scale height for all species. We assume that the atmospheric temperature T is uniform over the entire atmospheric column and horizontally constant across the disk. Doppler shifts produced by atmospheric winds (and Io's solid rotation of 75 m s^{-1} at the equator) are also included. While most dynamic models of Io's atmosphere predict a day-to-night global circulation driven by pressure gradients (Ingersoll 1989; Austin & Goldstein 2000), the only detection of planetary winds on Io showed a structure similar to a prograde zonal wind, which can also conveniently explain the observed width of rotational lines (Moullet et al. 2008). We hence introduce in our model a prograde zonal wind, characterized by the value of its equatorial velocity V, and for which, similarly to a solid rotation, velocity varies as a function of latitude as cos(lat). The projection of the zonal wind velocity on the line of sight is computed for each atmospheric column.

We use the minimum χ^2 method on a grid of parameters to estimate the best set of atmospheric parameters (d or χ, T, V) that can reproduce each observed line. The line contrast is mainly dependent on T and d, and if the lines are not saturated, the Doppler line width is mostly controlled by T and V. To break the possible degeneracy between retrieved parameters, when possible, we fit together different lines corresponding to distinct rotational transitions of the same molecule. Indeed, for a given molecule, the relative contrast between two lines of different intrinsic strength is mostly related to column density d, thus allowing for a quasi-independent determination of d. Here, by fitting altogether the absolute and relative line contrasts and widths on the two strong SO$_2$ lines at 346.523 and 346.652 GHz, we obtain an optimal solution for $d_{\rm SO_2}$ (or scaling parameter χ in the case of non-uniform distribution), allowing for a quasi-independent determination of T and V. Assuming that all species share the same T and V parameters and are co-located with SO$_2$, we can then independently adjust for each minor species disk-averaged column density (and hence mixing ratio q).

Table 2
Best-fit SO$_2$ Column Density (or Scaling Factor χ), Temperature, and Zonal Wind Velocity Assuming Homogeneous
and Feaga Distribution Models, for Different Portions of the Dataset

Date	Central Longitudes	Homogeneous Model			Feaga Model		
	($^\circ$W)	Column Density (10^{16} mol cm^{-2})	Temperature (K)	Wind Speed (km s^{-1})	Scaling Factor	Temperature (K)	Wind Speed (m s^{-1})
Combined		0.55	220	230	0.9	260	150
2010 Aug 20	90–114	0.65	280	180	0.9	350	60
2010 Aug 20	115–150	0.65	240	240	0.7	320	140
2010 Aug 20	90–150	0.70	230	250	0.8	330	130
2010 Aug 21	293–315	0.50	190	110	1.1	220	40
2010 Oct 13	279–312	0.65	150	110	0.9	190	40
2010 Oct 15	300–329	0.35	260	90	0.9	290	20
2010 Oct 13–15	279–312/300–329	0.45	190	170	0.9	300	20

3.3. Volcanically Sustained Case

To investigate the possible role of volcanism for minor species (SO, KCl, SiO, and S$_2$O), we use a different atmospheric model than the one described above, based on realistic models of gaseous plumes in a rarefied environment developed by Zhang et al. (2003) to simulate a plume-sustained atmosphere (see details in Moullet et al. 2008). These models do not include a background sublimation-sustained SO$_2$ component, so they only represent the direct volcanic contribution to the atmosphere.

The plume models fix the temperature and wind fields within a volcanic plume, as well as the spatial distribution of SO$_2$, corresponding to a canopy-shaped ballistic structure. The SO$_2$ total content in the plume, which ultimately relates to the SO$_2$ production rate from the vent, is also fixed so as to match SO$_2$ column densities measured over plumes by McGrath et al. (2000) and Jessup et al. (2004). Two types of plumes are considered corresponding to those identified on Io (McEwen & Soderblom 1983): Pele-type plumes, which are very large ($\sim$600 km radius) and rather rare, and the more common Prometheus-type ($\sim$200 km radius). Hence, the SO$_2$ emission from a given plume type (Prometheus or Pele) is entirely specified from the plume model (with no free parameters). Within each plume, the only adjustable parameter is the minor species mixing ratio q in the plume. By using a single q parameter for the whole plume, we hence assume that SO$_2$ and all other species share the same spatial distribution in the plume.

The total volcanic emission from an observed hemisphere can be modeled using a variable number of simultaneously active plumes of each category, placed at different locations on the disk. Our radiative transfer model allows simulation of any specified distribution of such plumes. In particular, we consider as the reference plume distribution the case where all plumes observed and localized by Galileo are active (Geissler & Goldstein 2007). This reference distribution includes 16 plumes, concentrated in particular on the anti-Jovian side, two of which being Pele-type plumes while the others are Prometheus-type plumes. The corresponding volcanically sustained atmospheric distribution hence exhibits large spatial variations of temperature and column density across the disk.

Volcanic models are used here to fit the SO, KCl, and SiO observations, using different plausible plume distributions, ranging from the most favorable case (reference plume distribution) to a minimal case where only one small plume near the sub-Earth point is active. For each plume distribution case, we determine the best-fitting q parameter in plumes that would be needed to reproduce the observed line contrast (or the upper limit on line contrast). The range of retrieved q parameters is then compared, for each species, to the range of mixing ratios predicted by thermochemical equilibrium models of volcanic gas chemistry. The goal eventually is to determine what fraction of the minor species' atmospheric content can plausibly be directly sustained by active volcanic plumes.

4. SO$_2$ AND SO: LONGITUDINAL DISTRIBUTION

4.1. SO$_2$

As measured on the combined spectrum (average of all obtained scans), the two SO$_2$ lines at 346.652 and 346.523 GHz offer a peak signal-to-noise ratio (S/N) of 14 and 10 per spectral channel, respectively. The best-fitting parameters obtained with the extended atmosphere models are gathered in Table 2 (line "combined"). For the homogeneous distribution model, we derive a column density $d = 5.5(\pm0.7) \times 10^{15}$ mol cm^{-2}, a temperature $T = 220 \pm 20$ K, and a wind velocity $V = 230 \pm 30$ m s^{-1}.

The addition of a prograde wind appears to be necessary to reach a satisfactory fit, and the V values found are compatible with the direct wind measurement of Moullet et al. (2008). The T values retrieved are typical of findings from (sub)millimeter and UV spectral data (Jessup et al. 2004), but higher than the upper limit derived from IR data ($\sim$160 K, Tsang et al. 2012). The data are also well reproduced for a column density distribution very similar to the Feaga model ($\chi = 0.9$). We notice that the disk-averaged column density in our rescaled Feaga model is somewhat higher than the value for a homogeneous distribution (8.3 versus 5.5 $\times$ 10^{15} mol cm^{-2}), since the former contains higher-density regions in which lines are saturated. The best model for a homogeneous atmospheric distribution is plotted against the observed lines in Figure 1.

For these strong SO$_2$ lines, the quality of the data is sufficient to split the data set into five portions covering $\sim$30° of rotational phase each (see Table 2). The same modeling approach was performed on each portion in order to estimate atmospheric longitudinal variations. On these shorter data sets, uncertainties on the best-fitted parameters reach $\sim$1.2 $\times$ 10^{15} mol cm^{-2} on d, 40 K on T, and 50 m s^{-1} on V. Comparing the results obtained on different dates, it is not straightforward in this data set to distinguish between longitudinal and temporal variations, as the data were obtained on two observation runs three months apart. The only direct temporal comparison can be done between the August 21 and October 13 data sets, which span approximately the same longitudes and give compatible modeling results.
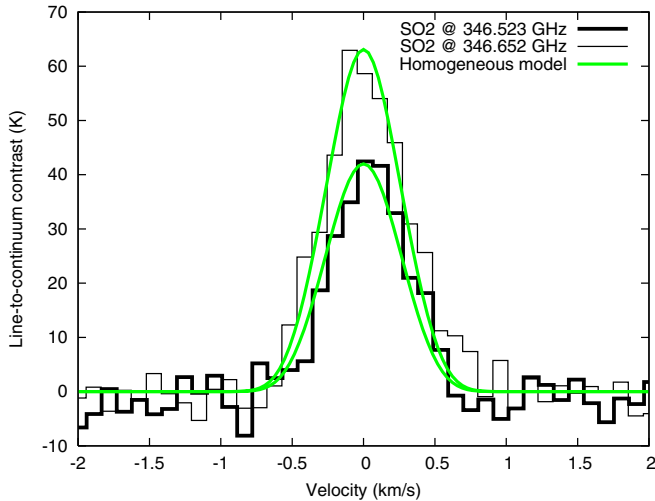
Figure 1. SO$_2$ lines measured on the combined spectrum (average of all scans), plotted against the best synthetic line models for a homogeneous atmospheric distribution.

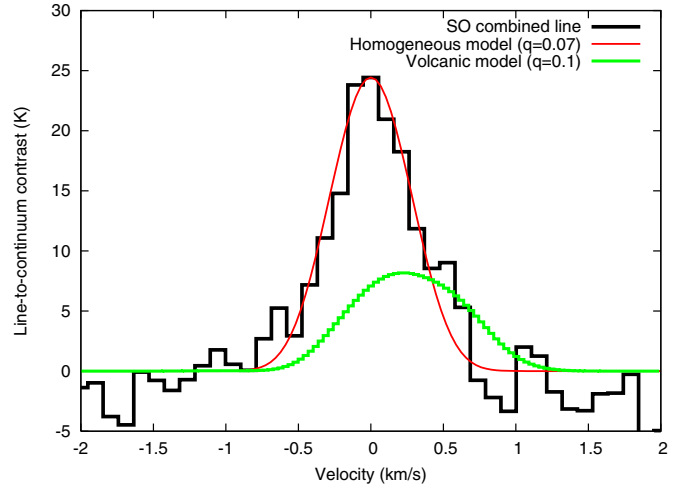(A color version of this figure is available in the online journal.)

Figure 2. Average of the two SO lines measured on the combined spectrum, plotted against the best synthetic line model for a homogeneous atmospheric distribution and for a volcanic model assuming the reference plume distribution and $q_{SO} = 0.1$. The volcanic model line appears to be slanted toward redshifted velocities, as it is dominated by the emission of plumes' infalling gas.

(A color version of this figure is available in the online journal.)

SO$_2$ disk-averaged column densities on both hemispheres appear to be of the same order, although they tend to be smaller on the trailing hemisphere than on the leading hemisphere. With scaling factors χ between 0.7 and 1.1, our rescaled Feaga models roughly follow the longitudinal column density variation trend proposed by the original Feaga distribution model. We find the only significant departure from the original Feaga model between central longitudes 90°W and 150°W, where our best models propose a quasi-constant disk-averaged column density, while the original Feaga model displays a ∼20% increase.

The prograde wind velocities appear to be systematically higher on the leading hemisphere than on the trailing hemisphere, where, at least for the case of rescaled Feaga models, the addition of a zonal wind is actually not required to provide a good fit. We note that a prograde zonal wind has been directly observed only on the leading hemisphere (Moullet et al. 2008).

Temperatures tend to be lower on the trailing hemisphere than on the leading hemisphere, with the exception of the high temperatures obtained for the October 15 data set. This particular dataset spans a large portion of the sub-Jovian hemisphere where lower SO$_2$ column densities (by a factor of two to four) are measured, a predicted consequence of daily eclipses (Feaga et al. 2009; Walker et al. 2012) which may make it more sensitive to plasma collisional heating (Wong & Smyth 2000).

4.2. SO

To derive the SO mixing ratio, we average on a common velocity scale the 344.310 and 346.528 GHz SO lines measured on the combined spectrum, assigning an equal weight to each transition. On the resulting averaged line, an S/N of nine per channel is reached on the line contrast (Figure 2). We consider the atmospheric models discussed in Section 3.2 and assume that SO and SO$_2$ are co-located. For a rigorous comparison, the radiative transfer code is run for both SO transitions, and the two obtained synthetic SO lines are averaged before being compared to the average observed SO line.

We find the best line fit for an SO mixing ratio of $q = 0.07 \pm 0.007$ (homogeneous distribution) or $q = 0.06 \pm 0.007$ (rescaled Feaga distribution), corresponding to a disk-averaged SO column density of, respectively, 3.8 and 4.5 × 10^{14} mol cm^{-2}. Given the data quality, it is possible to split

the data into three different portions—August 20, August 21, and October (13 and 15)—to look for mixing ratio variations. The values found (respectively, $q = 0.06$, 0.05, and 0.08 for the homogeneous case), given the error bars (∼0.012), do not support significant mixing ratio variations and are compatible with a scenario where SO is continuously present and detectable in the atmosphere.

These values fall in the mixing ratio range derived from previous (sub)millimeter observations ($q = 0.03$–0.1; Lellouch et al. 1996; Moullet et al. 2010). The assumption on co-location between SO and SO$_2$ in our extended atmosphere models could correspond to the case of SO being entirely sustained by SO$_2$ photolysis, for which SO mixing ratios lower than 0.15 are indeed predicted (Summers & Strobel 1996). However, several arguments in favor of an additional volcanic source for SO have been proposed, including a more localized and plume-linked distribution for SO compared to SO$_2$ (Moullet et al. 2010) and the detection of temporal mixing ratio variations (de Pater et al. 2007).

While our disk-averaged spectrum does not carry information on SO spatial distribution, we can investigate the possibility of a purely volcanically sustained SO atmosphere with our volcanic models. As explained in Section 3.3, we assume plausible plume distributions and derive the SO mixing ratio in plumes needed to reproduce the observed SO line. Assuming the most favorable case where all known plumes are active (reference plume distribution), the line contrast observed is reached for $q_{SO} = 0.7$, which is a much larger value than the mixing ratios predicted from volcanic thermochemical models (<10%, e.g., Zolotov & Fegley 1998). Consequently, even higher SO mixing ratios would be required if fewer plumes were active. These results demonstrate that the SO content measured in our observations cannot be entirely sustained by plume activity, at least in the context of the latest thermochemical models. To determine an upper limit to the volcanic contribution to SO total content, we simulate the emission produced in the most favorable yet realistic volcanic case, by fixing the SO mixing ratio in the plumes at $q = 10\%$ (corresponding to the upper range of predicted mixing ratios) and using the reference plume distribution. We then find that within our
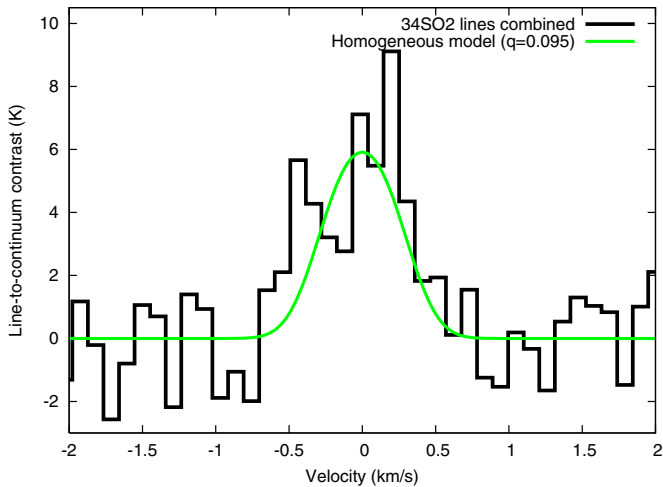
Figure 3. Average of the five $^{34}SO_2$ lines measured on the combined spectrum, plotted against the best synthetic line models for a homogeneous atmospheric distribution.

(A color version of this figure is available in the online journal.)

assumptions on realistic SO abundance and plume distribution, volcanic SO emission could only explain up to 30% of the total emission observed. Hence, our data are in agreement with the interpretation of previous (sub)millimeter observations, in which direct volcanic input of SO can only sustain a fraction of the SO content in the atmosphere, while SO_2 photolysis is the main source for SO.

5. NEW DETECTIONS AND UPPER LIMITS

5.1. First Detection of Gaseous $^{34}SO_2$

While the most common isotope of sulfur, ^{32}S, has been repeatedly detected in both solid and gaseous compounds, the sulfur isotopic composition has been only poorly constrained. A detection of the second-most common sulfur isotope (^{34}S) was only reported once, in a 4 μm $^{34}SO_2$ frost band (Howell et al. 1989). However, the $^{34}S/^{32}S$ ratio could not be derived, as the observed bands of $^{32}SO_2$ were too saturated to directly compare band depths.

To attempt the first determination of the $^{34}S/^{32}S$ ratio on Io, we averaged on a common velocity scale five different rotational lines of $^{34}SO_2$ that were each marginally detected on the combined spectrum, assigning an equal weight to each transition. The resulting average line is detected with an S/N of ∼4 on the line contrast (Figure 3). In a similar way as for SO, the data are compared to the average of the same five $^{34}SO_2$ synthetic lines produced by the radiative transfer code. The best $^{34}SO_2/^{32}SO_2$ ratio derived is of 0.095 ± 0.015, assuming a homogeneous distribution, and 0.08 ± 0.015, assuming the rescaled Feaga distribution.

5.2. Tentative Detection of KCl

The 344.820 GHz KCl line is tentatively detected (Figure 4). At the original spectral resolution (top panel), an S/N per channel of just ∼2 is reached; however, when the data are spectrally binned down to a resolution of 488 kHz, corresponding to ∼half the line width (middle panel), an S/N of 3 per channel is reached.

Assuming that SO_2 and KCl are co-located (extended atmosphere model), the KCl line is well modeled using a KCl mixing ratio of (5 ± 2) × 10⁻⁴, assuming a homogeneous distribution and (4 ± 2) × 10⁻⁴ for a rescaled Feaga distribution, both
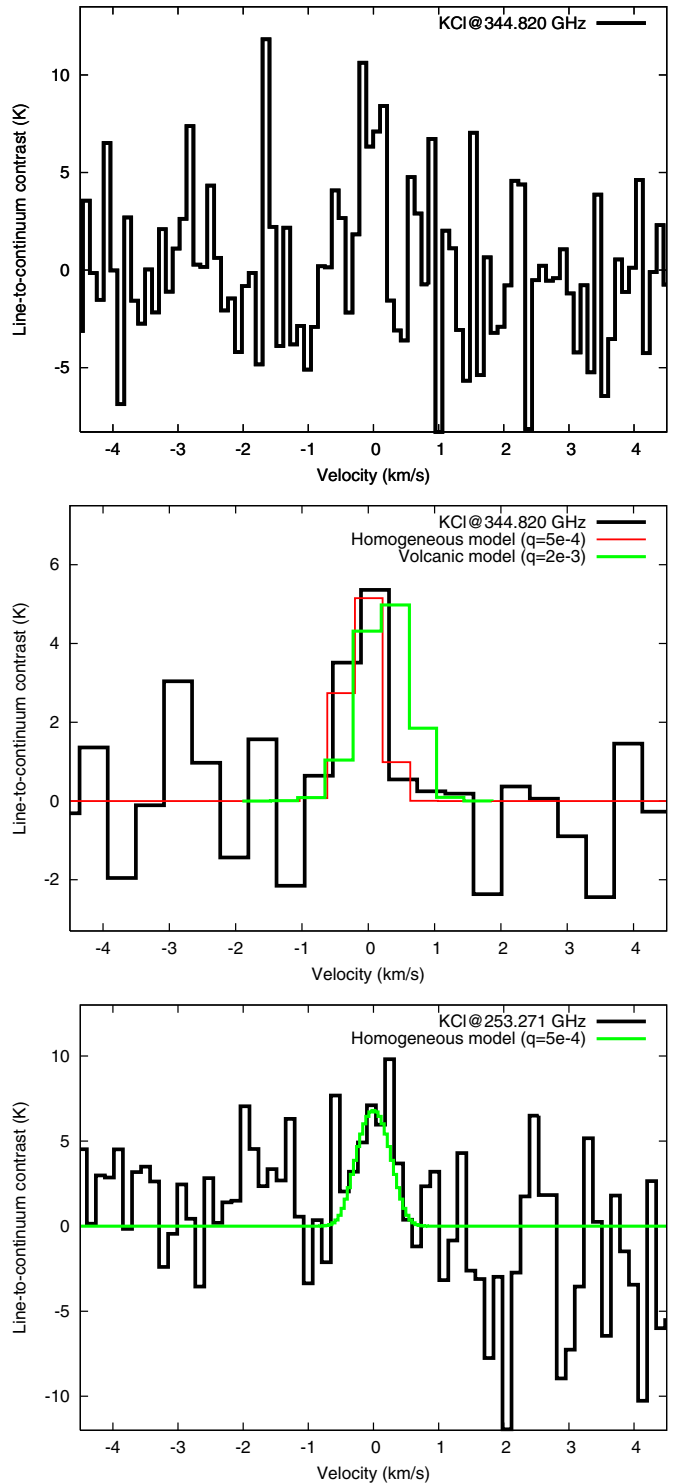

Figure 4. Top: KCl line tentatively detected at APEX with the original spectral resolution. Middle: KCl line tentatively detected at APEX (with a spectral resolution degraded to 488 kHz), plotted against the best models for a homogeneous atmospheric distribution ($q = 5 \times 10^{-4}$) and a purely volcanic model ($q = 2 \times 10^{-3}$ in plumes). Bottom: KCl line tentatively detected at IRAM 30 m (Lellouch et al. 2003), plotted against the homogeneous atmospheric distribution model.

(A color version of this figure is available in the online journal.)

corresponding to a KCl disk-averaged column density of ∼(3 ± 1) × 10¹² mol cm⁻².

To explore the case of a purely volcanic origin for KCl, we derived the range of KCl mixing ratios in plumes that is

compatible with the data, as explained in Section 3.3. In the most favorable situation where all known plumes are erupting (reference plume distribution), a KCl mixing ratio as low as 2×10^{-3} is sufficient. With such a distribution, the major part of the line emission is produced by the two large Pele-type Tvashtar and Pele plumes. Due to their geographic location (high northern latitudes on the leading hemisphere for Tvashtar, and as close as $15°$ from the western terminator on the trailing hemisphere for Pele), these plumes appear near the limbs, which is the geometry that most enhances the line emission. With a single erupting Pele plume near the sub-earth point (or 5 to 10 active Prometheus plumes distributed across each hemisphere), a KCl mixing ratio of 8×10^{-3} in plumes would be needed. With fewer active plumes, the observed contrast cannot be reached, as the KCl line saturates for mixing ratios higher than 8×10^{-3}.

The extended atmospheric model proposed above also reproduces the contrast of the 253.271 GHz KCl line tentatively detected at the IRAM 30 m antenna on 2002 January (see Figure 4, bottom panel; Lellouch et al. 2003). Those observations were interpreted, based on the comparison with NaCl lines, as a maximum KCl/NaCl ratio of 1 for an NaCl mixing ratio of $(2.5–5) \times 10^{-4}$ (corresponding to a maximum disk-averaged KCl column density of $(2.75–5.5) \times 10^{12}$ mol cm^{-2} assuming that all species are co-located). While the column density values appear to be consistent with the result obtained with our extended atmosphere model, a direct comparison of KCl mixing ratios cannot be drawn as the SO$_2$ atmospheric model used in Lellouch et al. (2003) is quite different from our model; in particular, it proposes a spatially concentrated and denser atmosphere to account for the large line widths, as opposed to a global atmospheric distribution in our models.

5.3. Upper Limits on SiO and S$_2$O

The search for the strong 347.330 GHz SiO line was unsuccessful. With an rms of 2 K on the spectrally binned data, the 3σ upper limit on the SiO mixing ratio is of $\sim 1.3 \times 10^{-3}$ for a homogeneous distribution and $\sim 0.8 \times 10^{-3}$ for a rescaled Feaga distribution, corresponding to an upper limit on the disk-averaged column density of $\sim 7 \times 10^{12}$ mol cm^{-2}.

We used volcanic models to determine a range of SiO mixing ratios in plumes that would just reach the measured upper limit on the line contrast, assuming that SiO is purely maintained in the atmosphere by active plumes. In the most favorable case (reference plume distribution), the upper limit would be reached for an SiO mixing ratio in plumes of 6×10^{-3}. With a single Pele plume near the sub-Earth point, a mixing ratio of 2×10^{-2} would be required, and with a single Prometheus plume, a mixing ratio of 0.7.

Finally, even when averaging the five spectral regions where S$_2$O transitions are expected within our observed spectral windows, S$_2$O could not be detected, only allowing us to a put a very loose mixing ratio upper limit of $q \sim 0.6$.

6. DISCUSSION

6.1. Interpretation of the ^{34}S/^{32}S Isotopic Ratio Result

The main observational result in this paper is the first reported detection of an ^{34}S-bearing molecule in gas phase. The range of values that we derive for the ^{34}S/^{32}S abundance ratio (within error bars, 0.065–0.120) is surprisingly higher than what was expected, as compared with the solar system reference ^{34}S/^{32}S value of 0.044 (Lodders 2003). While Howell et al. (1989) could not estimate the ^{34}S/^{32}S abundance ratio, they detected an ^{33}SO$_2$

band that allowed them to measure the ^{33}S/^{34}S abundance ratio in the solid phase to be 0.13 ± 0.07. This result is consistent with the solar system reference value (0.18; Lodders 2003), suggesting that the global sulfur isotopic composition on Io may be similar to the solar system reference.

Our measurement of the ^{34}S/^{32}S abundance ratio in the gas phase appears to be roughly twice as high as the solar system reference, as well as solar and interstellar medium values (Asplund et al. 2009; Lucas & Liszt 1998). An ^{34}S/^{32}S abundance ratio as high as our measurement has actually only been reported in redshifted absorption at $z \sim 0.89$ toward a quasar (Muller et al. 2006).

There are different ways to understand our result, depending on how and where fractionation occurs. First, the atmospheric ^{34}S enrichment observed may directly reflect the sulfur isotopic composition in Ionian magmas. This could be the same as the Ionian bulk sulfur isotopic distribution, or result from fractionation occurring within the lava. ^{34}S isotopic anomalies have been reported in terrestrial volcanic rocks and are thought to be linked to variations in magma temperature and composition (Marini et al. 1994; Sakai et al. 1982). Anomalies have also been measured in chondrites, achondrites, and iron meteorites (Gao & Thiemens 1993a, 1993b; Rai et al. 2005; Gao & Thiemens 1991). However, the anomalies reported in terrestrial and meteoritical materials are at most a few per hundred.

Another possibility is that mass-independent fractionation processes at work in the atmosphere significantly change the gas-phase isotopic composition with respect to the solid-phase isotopic distribution. SO$_2$ photolysis, chemical reactions, and atmospheric transport have, for example, all been invoked to explain the enrichment in ^{34}S observed in some terrestrial volcanic gases (Farquhar et al. 2001; Baroni et al. 2007), although the isotopic anomalies reported and modeled in those cases are of the order of a few per thousand only.

Finally, since the immediate source of SO$_2$ is dominated by sublimation equilibrium, it could be possible that sublimation/condensation cycles produce mass-dependent fractionation between ^{32}SO$_2$ and ^{34}SO$_2$, which are expected to have slight differences in equilibrium vapor pressure. These three possibilities may all be important to varying degree, but remain speculative and require quantitative evaluation to verify if they could account for the ^{34}S enrichment that we measure.

6.2. Potassium Chloride

The accumulation of tentative detections of KCl (sub) millimeter lines is an encouraging sign for definitive KCl detection using more sensitive instruments. The presence of K-bearing molecules in Io's atmosphere is strongly anticipated, as K atoms are suspected to be present in the upper atmosphere based on the spectral analysis of UV airglows observed by Cassini (Geissler et al. 2004) and have been detected in Io's corona (Brown 2001). In addition, K atoms and K-bearing dust have been detected, respectively, in Io's neutral clouds (Trafton 1975) and in Jupiter's rings (Postberg et al. 2006), which are both believed to be ultimately fed by Io's atmosphere. Using terrestrial volcanism analogies, Fegley & Zolotov (2000a), Moses et al. (2002), and Schaefer & Fegley (2004, 2005) suggest that potassium is originally present in Io's erupting magma, from which it is easily volatilized due to the high temperatures of volcanic regions and low atmospheric pressures. KCl is the expected main K carrier in these models and could be injected to the atmosphere directly from volcanic vents. Assuming Cl/S and K/S abundance ratios of 0.045 and 0.005,

respectively, Schaefer & Fegley (2005) predict a KCl mixing ratio in the plumes of $\sim 8 \times 10^{-3}$ for a wide range of conduit pressures. They also predict that KCl should have a short lifetime in the atmosphere (<2 hr) due to condensation and photolysis. In regions where the bulk atmosphere is thinner, for example because of low sublimation-sustained SO_2 (nightside), gaseous K-bearing molecules could also be produced by sputtering of volcanic-ash-coated surfaces by high-energy particles, in particular on the trailing hemisphere that is hit by plasma torus particles (Haff et al. 1981). In this context, most of the KCl content on the dayside should correspond to a short-lived volcanically sustained atmosphere, indicative of ongoing volcanic activity.

Our volcanic modeling results on KCl are consistent with this hypothesis. We have shown that assuming the KCl mixing ratio proposed by Schaefer & Fegley (2005) ($\sim 8 \times 10^{-3}$), a plausible distribution of active plumes could explain the tentatively detected KCl line. Our data are compatible with volcanism being the only KCl source on the dayside atmosphere.

Considering the plume distribution models proposed in Section 5.2 to explain the KCl tentative detection, we derive the corresponding total volcanically produced KCl. Given the SO_2 emission fluxes fixed by our individual plume models (1.1×10^4 kg s^{-1} for a Prometheus plume, 2.2×10^4 kg s^{-1} for a Pele plume), we estimate a production rate ranging between 7.8×10^9 and 4×10^{10} KCl molecules s^{-1} cm^{-2} (accounting for the emission from both hemispheres). We can compare this result to atmospheric escape rates measured at higher altitudes. Mendillo et al. (2004) measured the Na escape rate during volcanically active periods to be in the range $(1.8$–$5.6) \times 10^9$ Na atoms s^{-1} cm^{-2}. Assuming the Na/K ratio measured in the corona by Brown (2001) (10 ± 3), the K atom escape rate inferred is of one to two orders of magnitude lower than our proposed volcanic KCl production rate. Our models are compatible with volcanically produced KCl in Io's bulk atmosphere being the sole source of K atoms for the corona. This result is consistent with the general behavior that atmospheric escape represents only a small fraction of the volcanic output, and in particular with the 50–100 times larger NaCl volcanic input compared to the upward flux of atomic Na and Cl at the top of the atmosphere (Moses et al. 2002; Lellouch et al. 2003).

In addition to these results on the possible contribution of volcanism to atmospheric KCl content, our data allow us to constrain the Na/K atmospheric ratio. As explained in Schaefer & Fegley (2004), obtaining a stringent determination of the Na/K ratio in the bulk atmosphere can be a powerful tool to distinguish between different types of lavas (silicate, basalt, K-rich) and constrain vaporization temperature. In the lower atmosphere, where most of gaseous K and Na is believed to be carried in KCl and NaCl, respectively (Fegley & Zolotov 2000a; Moses et al. 2002; Schaefer & Fegley 2005), this can be done by measuring the NaCl/KCl ratio. Our observed spectral windows did not include NaCl transitions that would allow a direct comparison. Using the 338.021 GHz NaCl line detected at the Sub Millimeter Array (SMA, Moullet et al. 2010), we derive disk-averaged NaCl column densities in the range $(7$–$9) \times 10^{-12}$ mol cm^{-2}, leading to an NaCl/KCl ratio of $2.7^{+1.8}_{-1}$.

This result is consistent with and close to the Na/K value proposed for the upper atmosphere by Geissler et al. (2004) (~ 3.3). Both these measurements are much lower, by several orders of magnitude, than most Na/K ratios modeled for gases vaporized over lavas that could be Ionian analogues (Schaefer & Fegley 2004), and significantly lower than cosmic and chondritic values (16 and 15, respectively; Asplund et al. 2009; Lodders

2003). Schaefer & Fegley (2004) address this issue in detail by proposing that since Na is more volatile than K, fractional vaporization effects could over time lead to a depletion of the Na content in lavas and therefore in the atmosphere. Another proposition is the presence of originally K-rich lavas (ultra-potassic lavas with Na/K down to ~ 2.8).

We also note that our Na/K estimate is lower than the value measured in the corona based on Na and K atoms (10 ± 3, Brown 2001). This apparent Na/K ratio increase from the bulk atmosphere to Io's environment needs to be confirmed by higher-precision measurements, as it would be indicative of processes acting differently on K-bearing and Na-bearing molecules and atoms. Brown (2001) actually argues that their corona measurement should be considered as an upper limit on the Na/K ratio near the surface, as K atoms are more quickly photo-ionized than Na atoms.

6.3. Silicon Oxide

The present understanding of Io's volcanism is that both silicate-based and sulfur-based magmas are driving volcanic activity (Williams & Howell 2007). The very high temperatures measured in some volcanic regions (Lopes-Gautier et al. 1999) are much higher than the sulfur boiling point but consistent with silicate flows akin to those commonly found on Earth (basalts), or to ultra-mafic lavas (McEwen et al. 1998). The rigidity of the surface topographic features, including several kilometer-high mountains (Clow & Carr 1980), also points to a silicate-based crust that would explain Io's bulk density. While sulfur-bearing volatiles can be dissolved in silicate melts (Carr et al. 1979), the overall predominance of sulfur on Io's surface, atmosphere, and environment suggests the possibility of co-existent sulfur-based magmas. Most measured hot-spot temperatures are indeed low enough to be consistent with molten-sulfur magma (McEwen & Soderblom 1983), and the morphology of some bright volcanic regions is indicative of sulfur flows (McEwen et al. 2000). No Si-carrying molecules have been positively identified on Io, and such a detection would provide an additional strong proof of the existence of silicate volcanism on Io.

The science case behind the interpretation of SiO content is similar to that of KCl. Vaporization models show that SiO should be the main Si-bearing volatile over silicate lavas at very high temperature (Schaefer & Fegley 2004), and that it is expected to condense very quickly, so that its presence should be restricted to active volcanic plumes. However, unlike KCl, the amount of vaporized SiO depends strongly on lava temperature, with column densities above lavas expected to span four orders of magnitude (for a temperature range between 1700 and 2400 K). Based on the examples given in Schaefer & Fegley (2004), the SiO column density over a plume can vary between 2×10^{15} mol cm^{-2} and 8×10^{18} mol cm^{-2}. Considering that the SO_2 column density over Pele and Prometheus plumes is of the order of 2×10^{18} mol cm^{-2} based on plume-resolved measurements (Jessup et al. 2004; Spencer et al. 2000), this means a wide possible range for SiO mixing ratio in plumes from 1×10^{-3} to 4.

Our modeling shows that it is possible to reproduce our measured upper limit on the SiO line for a variety of plausible plume distributions, assuming mixing ratios in the range of 6×10^{-3}–0.7, which are within the range of predicted SiO mixing ratios. Hence, our upper limit measurement is entirely consistent with a purely volcanic source for SiO.

Using the same results presented above on NaCl content, and given that SiO is expected to be the main Si carrier, we derive

an upper limit on the Si/Na ratio of ~1. This value is much less stringent than the value obtained by Na et al. (1998) on the Si/Na ratio in the corona (0.014). Our upper limit also appears to be consistent with the Si/Na ratio measured in the vaporized phase above most terrestrial basalts (of the order of 1×10^{-3}–1×10^{-6}; Schaefer & Fegley 2004), but is too imprecise to constrain lava composition.

7. CONCLUSIONS

This work demonstrates how (sub)millimeter observations can be used to derive unique constraints on the composition and sources of Io's lower atmosphere, which are essential to understand Io's volcanism and atmospheric processes, but also demonstrates the sensitivity limits reached by APEX observations that prevent us from performing spectroscopic searches deep enough to detect further minor species. In particular, obtaining better upper limits on volcanic tracers such as SiO would strongly constrain the characterization of Ionian volcanic regimes. In addition, the interpretation of disk-averaged spectra of a strongly spatially variable atmosphere is inherently uncertain, and in particular for optically thick lines, the necessary assumptions on spatial distribution can lead to significantly different results in column density. With an apparent size of $0\rlap{.}''9$–$1\rlap{.}''2$, the use of interferometric facilities is necessary to resolve Io's disk, and observations with the SMA and IRAM-PdBI offer a spatial resolution down to $0\rlap{.}''4$ allowing for a first-order assessment of atmospheric coverage.

The Atacama Large Millimeter Array (ALMA), a 64-element array that is approaching completion near the APEX site, will provide the necessary boosts in sensitivity and spatial resolution. Due to its very large collecting area and state-of-the-art receivers, detection limits on minor species could be lowered by a factor of ~50–70, allowing for searches of more species and isotopes. Extended array configurations could be used to reach spatial resolution down to $0\rlap{.}''15$ (corresponding to ~400–500 km, i.e., the size of a Prometheus-type plume) with a sufficient S/N at ~350 GHz, allowing direct determination of the local SO_2 column density as well as helping to establish the link between atmospheric species and their respective sources. ALMA observations are then one of the most promising prospects in the next decade for the advancement of the understanding of Io at large.

REFERENCES

Asplund, M., Grevesse, N., Sauval, A. J., & Scott, P. 2009, ARA&A, 47, 481
Austin, J. V., & Goldstein, D. B. 2000, Icar, 148, 370
Baroni, M., Thiemens, M. H., Delmas, R. J., & Savarino, J. 2007, Sci, 315, 84
Brown, M. E. 2001, Icar, 151, 190
Carr, M. H., Masursky, H., Strom, R. G., & Terrile, R. J. 1979, Natur, 280, 729
Chrisey, D. B., Johnson, R. E., Boring, J. W., & Phipps, J. A. 1988, Icar, 75, 233
Clow, G. D., & Carr, M. H. 1980, Icar, 44, 268
de Pater, I., Laver, C., Marchis, F., Roe, H. G., & Macintosh, B. A. 2007, Icar, 191, 172
Farquhar, J., Savarino, J., Airieau, S., & Thiemens, M. H. 2001, JGR, 106, 32829
Feaga, L. M., McGrath, M., & Feldman, P. D. 2009, Icar, 201, 570
Fegley, B., & Zolotov, M. Y. 2000a, Icar, 148, 193
Fegley, B., Jr., & Zolotov, M. Y. 2000b, M&PSA, 35, 52
Gao, X., & Thiemens, M. H. 1991, GeCoA, 55, 2671
Gao, X., & Thiemens, M. H. 1993a, GeCoA, 57, 3159
Gao, X., & Thiemens, M. H. 1993b, GeCoA, 57, 3171
Geissler, P., McEwen, A., Porco, C., et al. 2004, Icar, 172, 127
Geissler, P. E., & Goldstein, D. B. 2007, in Io After Galileo: A New View of Jupiter's Volcanic Moon, ed. R. M. C. Lopes & J. R. Spencer (Berlin: Springer Praxis Books), 163
Güsten, R., Nyman, L. Å., Schilke, P., et al. 2006, A&A, 454, L13
Haff, P. K., Watson, C. C., & Yung, Y. L. 1981, JGR, 86, 6933
Howell, R. R., Nash, D. B., Geballe, T. R., & Cruikshank, D. P. 1989, Icar, 78, 27
Ingersoll, A. P. 1989, Icar, 81, 298
Jessup, K. L., Spencer, J. R., Ballester, G. E., et al. 2004, Icar, 169, 197
Johnson, M. L., & Burnett, D. S. 1990, GeoRL, 17, 981
Klein, B., Philipp, S. D., Krämer, I., et al. 2006, A&A, 454, L29
Lapkin, I., Nyström, O., Desmaris, V., et al. 2008, in Ninteenth International Symposium on Space Terahertz Technology, ed. W. Wild (Groningen: SRON), 351
Lellouch, E. 2005, SSRv, 116, 211
Lellouch, E., Paubert, G., Moses, J. I., Schneider, N. M., & Strobel, D. F. 2003, Natur, 421, 45
Lellouch, E., Strobel, D. F., Belton, M. J. S., et al. 1996, ApJL, 459, L107
Lodders, K. 2003, ApJ, 591, 1220
Lopes-Gautier, R., McEwen, A. S., Smythe, W. B., et al. 1999, Icar, 140, 243
Lucas, R., & Liszt, H. 1998, A&A, 337, 246
Marini, L., Paiotti, A., Principe, C., Ferrara, G., & Cioni, R. 1994, BVol, 56, 487
McEwen, A. S., Belton, M. J. S., Breneman, H. H., et al. 2000, Sci, 288, 1193
McEwen, A. S., Keszthelyi, L., Spencer, J. R., et al. 1998, Sci, 281, 87
McEwen, A. S., & Soderblom, L. A. 1983, Icar, 55, 191
McGrath, M. A., Belton, M. J. S., Spencer, J. R., & Sartoretti, P. 2000, Icar, 146, 476
Mendillo, M., Wilson, J., Spencer, J., & Stansberry, J. 2004, Icar, 170, 430
Moses, J. I., Zolotov, M. Y., & Fegley, B. 2002, Icar, 156, 107
Moullet, A., Gurwell, M. A., Lellouch, E., & Moreno, R. 2010, Icar, 208, 353
Moullet, A., Lellouch, E., Moreno, R., Gurwell, M. A., & Moore, C. 2008, A&A, 482, 279
Muller, S., Guélin, M., Dumke, M., Lucas, R., & Combes, F. 2006, A&A, 458, 417
Müller, H. S. P., Schlöder, F., Stutzki, J., & Winnewisser, G. 2005, JMoSt, 742, 215
Na, C. Y., Trafton, L. M., Barker, E. S., & Stern, S. A. 1998, Icar, 131, 449
Postberg, F., Kempf, S., Srama, R., et al. 2006, Icar, 183, 122
Rai, V. K., Jackson, T. L., & Thiemens, M. H. 2005, Sci, 309, 1062
Sakai, H., Casadevall, T. J. C., & Moore, J. G. 1982, GeCoA, 46, 729
Schaefer, L., & Fegley, B. 2004, Icar, 169, 216
Schaefer, L., & Fegley, B. 2005, Icar, 173, 454
Schneider, N. M., & Bagenal, F. 2007, in Io After Galileo: A New View of Jupiter's Volcanic Moon, ed. R. M. C. Lopes & J. R. Spencer (Berlin: Springer Praxis Books), 265
Spencer, J. R., Jessup, K. L., McGrath, M. A., Ballester, G. E., & Yelle, R. 2000, Sci, 288, 1208
Spencer, J. R., Lellouch, E., Richter, M. J., et al. 2005, Icar, 176, 283
Summers, M. E., & Strobel, D. F. 1996, Icar, 120, 290
Trafton, L. 1975, Natur, 258, 690
Tsang, C. C. C., Spencer, J. R., Lellouch, E., et al. 2012, Icar, 217, 277
Walker, A. C., Moore, C. H., Goldstein, D. B., Varghese, P. L., & Trafton, L. M. 2012, Icar, 220, 225
Wiens, R. C., Burnett, D. S., Calaway, W. F., et al. 1997, Icar, 128, 386
Williams, D. A., & Howell, R. R. 2007, in Io After Galileo: A New View of Jupiter's Volcanic Moon, ed. R. M. C. Lopes & J. R. Spencer (Berlin: Springer Praxis Books), 265
Wong, M. C., & Smyth, W. H. 2000, Icar, 146, 60
Zhang, J., Goldstein, D. B., Varghese, P. L., et al. 2003, Icar, 163, 182
Zolotov, M. Y., & Fegley, B. 1998, Icar, 132, 431